

Acoustic Pyrometry System for Environmental Protection in Power Plant Boilers

S. P. Zhang, L. S. An*, G. Q. Shen, and Y. G. Niu

Key Laboratory of Condition Monitoring and Control for Power Plant Equipment Ministry of Education, North China Electric Power University, Beijing 102206, China

Received 17 September 2013; revised 24 October 2014; accepted 5 May 2014; published online 20 June 2014

ABSTRACT. On-line monitoring of the distribution of the temperature field in a boiler furnace is important to reduce emissions that cause pollution and damage to the environment in power plants. Acoustic pyrometry, which is best suited for high temperature and dusty conditions, has been a very active research area recently. The present study provides a reconstruction technique of a two-dimensional temperature field through the measurements of multiple paths, which is used to monitor the combustion process in the boiler furnace. The geometric pixel division and the regularization algorithm were used to solve the reconstruction problem of temperature profile in many cases. Then, adopting this method, a temperature field monitoring system with multiple paths was developed and applied to a 330 MW unit (opposed wall firing). Through the long-term operations, it was proved that the acoustic pyrometer system could realize the visualization of temperature profile in the furnace.

Keywords: on-line monitoring, temperature field, acoustic pyrometry, geometric pixel division, regularization algorithm

1. Introduction

The utility of industrial power plants is very important in today's electricity-dependent world, but coal-fired power generation is the leading source of carbon and other pollutants in the electric industry (Feron, 2010; Zhao et al., 2010). There has been a high level of environmental contamination from combustion emissions already, so energy saving and waste minimization of coal-fired power plants have become urgent problems (Pedersen et al., 2009; Popp, 2010; Thitakamol et al., 2007; Zhao et al., 2008). The distribution of the temperature field is one of the most important parameters to diagnose and monitor the combustion process in a boiler furnace (Wang et al., 2012). Hence, on-line monitoring of the temperature profile can help optimize the burning operation mode and improve the combustion efficiency. Furthermore, coal resources are saved, and pollutant emissions, such as NO_x and CO, are reduced (Cai et al., 2009). This will contribute to energy conservation and environmental protection.

For high temperature measurement techniques, there are two common measuring methods to use, which encompass contact and non-contact measurements. Contact measurements include thermocouple thermometers, pressure thermometers, blackbody chamber thermometers, and fiber temperature measuring systems (Frankel et al., 2010; Liu et al., 2000; Pullins

and Diller, 2010; Seat et al., 2002; Walker et al., 2000; Yu et al., 2010). Non-contact temperature measurements are divided into optical methods, which typically include radiation spectroscopy and laser spectroscopy, and acoustic methods, which include the velocity method and frequency method (Hoyle and Luke, 1994; Konno et al., 1993; Moll et al., 2010; Myers et al., 2013; Wadley et al., 1986; Yan et al., 2012; Zhu et al., 2010). Like thermocouples, the majority of contact measurements can only be used to measure the temperature of a point with a slower response, which do not realize the measurement of a temperature field and cannot be inserted into flue gas with high temperature for a long time (Gam, 1996; Sarma and Boruah, 2010). Non-contact temperature measurement by laser is an advanced method for measuring temperature, but larger power sources that are very expensive are required due to the large-scale boiler furnace. Because the laser travels in a straight line, the resolution of the temperature field is low unless more measuring points are installed, which will increase the cost (Doubenskaia et al., 2006). The method of infrared temperature surveying is commonly applied due to its many merits (Mahan and Yeater, 2008; Ranc and Wagner, 2005). In fact, due to the harsh environment in a furnace, this method cannot measure the temperature accurately. Optical measurement has a serious shortcoming, which is that the camera lenses can be smeared by the ash and affect the measurement result (Ballester and García-Armingol, 2010; Chen et al., 2010; Chi et al., 2010; Meriaudeau, 2007; Romero et al., 2005; Yan et al., 2002). The real-time monitoring of temperature based on acoustic pyrometry has many benefits, such as high resolution of temperature measurement, wide range, non-intrusive, real time monitoring, and low maintenance. It has become a

* Corresponding author. Tel.: +86 10 61772366; fax: +86 10 61772366.
E-mail address: liansuoan@gmail.com (L. S. An).

popular topic in temperature measurement (Jen et al., 2000; Srinivasan et al., 2013)

In the present study, we focused on the online monitoring of temperature profiles using acoustic measurement. The physical principle of acoustic pyrometry and the reconstruction algorithm of a two-dimensional spatial profile through the measurements of multiple paths are first discussed in Section 2. Next, the simulation test is designed to prove that the algorithm is feasible and accurate. In Section 3, the monitoring system of the temperature field sourced from this reconstruction technique is developed and applied to a 330 MW unit (opposed wall firing). And then, temperatures are verified by the thermocouple in particular regions. Conclusions are drawn in section 4.

2. Method and Simulation

2.1. Physical Principles of Acoustic Pyrometry

Sound waves are emitted by a sound source on one side and received by microphones on both sides, which are installed in the wall of a boiler furnace. First, loud sound can be generated by the sound source and it is received by the microphone near the source on one side. Then, the sound across the furnace is received by the microphone on the other side. Meanwhile, to calculate the acoustic velocity, time of flight (TOF) should be measured by estimating the time delay of sound wave transmission between the microphones. In a mixture of gases with a definite composition, such as boiler flue gas, the speed of the sound wave depends on the temperature of the gas. The principle equation of acoustic pyrometry is as follows:

$$c = \frac{L}{\tau} = \sqrt{\frac{\gamma R}{m} T} \quad (1)$$

where c is the speed of the acoustic wave propagation in the medium, L is the distance between the different measuring points, τ is the TOF, γ is the isentropic exponent of gas, R is the universal gas constant of an ideal gas, m is the molar mass, and T is the gas temperature. $Z = \sqrt{\gamma R / m}$ is a constant for a given gas mixture. The sound speed, which depends on the temperature of the medium and contains temperature variations, is obtained by measurement of the TOF. Hence, the calculation formula of the one-path temperature derived from the Formula (1) is as follows:

$$T = \left(\frac{L}{\tau Z}\right)^2 \quad (2)$$

2.2. Reconstruction Algorithm of the Two-dimensional Spatial Profile

In addition to the fundamental single path measurement, a number of acoustic wave generators and receivers can be placed around the perimeter of a furnace to obtain a multiple

paths array. The array contains side-to-side, front-to-back, and diagonal paths within the planar region of the furnace. For example, there are 24 paths formed by 8 acoustic measuring points in Figure 1. In every measuring point, the sound source and receiving device are installed. According to the designed program, each point is commanded to send sound signals in sequence, and the TOF over the various paths are acquired. Then, a two-dimensional spatial profile of the gas temperature distribution is created by computer and image reconstruction techniques. This is called visualization of the temperature field. The temperature profile is automatically updated every minute, and on-line continuous measurement is realized.

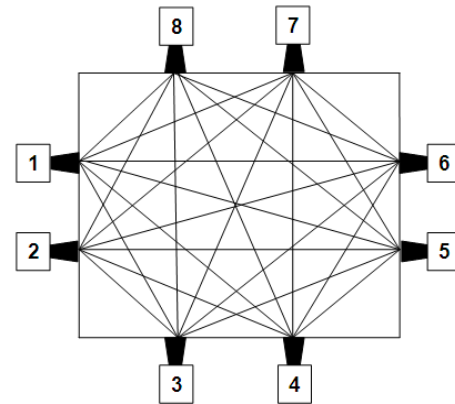


Figure 1. The 8 transceiver 24 paths.

There are two approaches generally used to describe the spatial profile of the temperature field. In one way, the section is discretized to obtain the temperature distribution of the different discrete units that are assumed to be uniform. Another way is to determine the unknown coefficients of the function that is used to describe the temperature profile in a furnace (Tarantola, 1987). In this paper, the first method was adopted.

The two-dimensional temperature field to be reconstructed is discrete and is divided into N non-overlapping regions of pixels, called geometric pixel division. The new temperature function is defined as follows:

$$f(x, y) = \frac{1}{\sqrt{\frac{\gamma R}{m} T}} = \frac{1}{v} \quad (3)$$

A linear operator R_i is proposed, as shown in the following equation:

$$\tau_i = \int_{\frac{1}{v}}^1 dl_i = R_i f(x, y) = \sum_{j=1}^N f_j w_{ij}, \quad i = 1, 2, \dots, M \quad (4)$$

where τ_i is the TOF, and w_{ij} is the weighted factor, which is equal to the length of ray i that goes through pixel j .

Hence, linear equations can be obtained after a period of

measured section is divided into 3×3 pixels, and the regularization matrix D can be expressed as:

$$D = \begin{bmatrix} 1 & -1/3 & 0 & -1/3 & -1/3 & 0 & 0 & 0 & 0 \\ -1/5 & 1 & -1/5 & -1/5 & -1/5 & -1/5 & 0 & 0 & 0 \\ 0 & -1/3 & 1 & 0 & -1/3 & -1/3 & 0 & 0 & 0 \\ -1/5 & -1/5 & 0 & 1 & -1/5 & 0 & -1/5 & -1/5 & 0 \\ -1/8 & -1/8 & -1/8 & -1/8 & 1 & -1/8 & -1/8 & -1/8 & -1/8 \\ 0 & -1/5 & -1/5 & 0 & -1/5 & 1 & 0 & -1/5 & -1/5 \\ 0 & 0 & 0 & -1/3 & -1/3 & 0 & 1 & -1/3 & 0 \\ 0 & 0 & 0 & -1/5 & -1/5 & -1/5 & -1/5 & 1 & -1/5 \\ 0 & 0 & 0 & 0 & -1/3 & -1/3 & 0 & -1/3 & 1 \end{bmatrix} \quad (16)$$

Generally speaking, the values of the regularization parameter α are not fixed, but it can be determined by a Newton or higher order convergence algorithm. To evaluate the value of α , a simulation experiment was conducted, which found that the value range of α was between 1 and 5, with little change of the temperature gradient.

1	2	3
4	5	6
7	8	9

Figure 3. Two-dimensional profile consists of 9 pixels.

Through the above reconstruction, a two-dimensional image that has 9 pixels can be obtained. Then, bicubic interpolation is proposed to obtain larger pixels.

2.4. Bicubic Interpolation

In the numerical analysis, the interpolation algorithm can be expressed as follows:

$$g(x) = \sum_{k=0}^{n-1} C_k \times h(x - x_k) \quad (17)$$

where $h(x - x_k)$ is the basis function of the interpolation, and C_k is the value of the k^{th} original function.

Bicubic interpolation is an effective way to be selected in a two-dimensional image, whose basic function has discontinuous first and second derivatives. Considering a good reconstructed image and low hardware cost, the cubic interpolation basis function propounded by Keys (Keys, 1981) was used in the acoustic pyrometry system. x_1, x_0, x_1 and x_2 are the known sample points in equal intervals, and x is the interpolating point of the solution. Assuming $h = x_1 - x_0$ and $s = (x_1 - x_0)/h$, the expression of the interpolation point is as follows:

$$f(x) = \sum_{k=-1}^2 f(x_k)u(s) \quad (18)$$

If h is normalized to 1, the basis function propounded by

Keys is described as follows:

$$u(s) = \begin{cases} \frac{3}{2}|s|^3 - \frac{5}{2}|s|^2 + 1 & 0 < |s| < 1 \\ -\frac{1}{2}|s|^3 + \frac{5}{2}|s|^2 + 2 & 1 < |s| < 2 \\ 0 & 2 < |s| \end{cases} \quad (19)$$

Hence, let us suppose that the interpolated pixel is F . First, according to the interpolation principle, each line can have 4 pixel values, which are $F_0, F_1, F_2,$ and F_3 ($F_i = \sum_{k=0}^3 f_{k+4i}u(\Delta x)$), where f_{k+4i} are the values of 16 nearby pixel points from the input image, and the distance between two pixel points is 1. Then, taking F_i as the basis function, in the vertical direction, the value of interpolation point F is exactly soluble according to the same principle, as shown in the following equation:

$$F = \sum_{k=0}^3 F_i \times (\Delta y) \quad (20)$$

2.5. Simulation Experiment

A measured rectangular section (15×14 m) was set above the burners in a unit of 300 MW, which was selected as the simulation object in a domestic power plant. The eight symmetrical acoustics points were adopted to form 24 paths (see Figure 1). The two-dimensional measured profile was evenly divided into $4 \times 4 = 16$ pixels, and it was supposed that the temperature distribution of each pixel was the same as the preconditions. According to the model of the temperature field, the TOF of sound over each measured path should be obtained through its line integral on the path, as shown in Equation 4, to obtain the temperature. However, in the application in the boiler furnace, the TOF is obtained by measurement through the time delay estimation algorithm. The models of the temperature field in the simulation were as follows:

Model of symmetry with one peak:

$$T = 800 + 1000 \cdot \sin\left(\frac{x}{15}\pi\right) \cdot \sin\left(\frac{y}{14}\pi\right) \quad (21)$$

Model of dissymmetry with one peak:

$$T = 1200 \cdot \exp\left(-\frac{(x-11)^2 + (y-7)^2}{100}\right) + 600 \quad (22)$$

Model of symmetry with two peaks:

$$T = 1100 \cdot \exp[-0.08(x-4)^2 + 0.05(y-7)^2] + 1100 \exp[-0.08 \times (x-11)^2 + 0.05(y-7)^2] + 700 \quad (23)$$

Model of dissymmetry with two peaks:

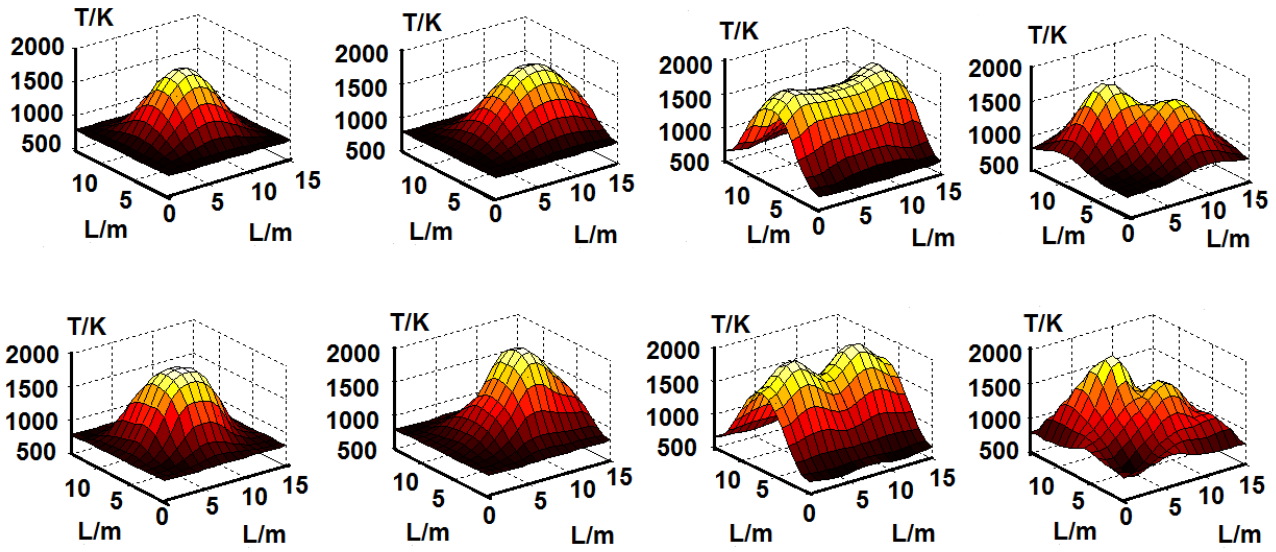


Figure 4. The simulation results of temperature field.

$$T = 800 + 1000 \cdot \exp[-20(\frac{x}{15} - \frac{1}{3})^2 - 20(\frac{y}{14} - \frac{2}{3})^2] + 600 \cdot \exp[-20 \times (\frac{x}{15} - \frac{2}{3})^2 - 15(\frac{y}{14} - \frac{1}{3})^2] \quad (24)$$

The temperatures of the 16 pixels were obtained through the regularized reconstruction algorithm mentioned above. Based on these data, the two-dimensional temperature of the measured rectangular section was reconstructed by 16×14 bicubic interpolation. The simulation results are in Figure 4. The models of the temperature fields are shown in Figures 4a1, 4b1, 4c1 and 4d1. The reconstructed temperature fields are illustrated in Figures 4a2, 4b2, 4c2 and 4d2. When the model of the temperature field is symmetry with one peak, the relative error is 3.89% and the mean square root error is 7.30%. When the model of the temperature field is dissymmetry with one peak, the relative error is 3.50% and the mean square root error is 7.63%. When the model of the temperature field is symmetry with two peaks, the relative error is 5.20% and the mean square root error is 6.97%. When the model of the temperature field is dissymmetry with two peaks, the relative error is 6.59% and the mean square root error is 7.46%. In the abovementioned simulations, the noise effect of the boiler furnace in the hot state was not considered. The noise would affect the measurement accuracy of the TOF and ultimately affect the accurate image reconstruction in practice. However, the time delay estimation algorithm could obtain accurate TOF and solve the problem. Moreover, under consideration of the abovementioned factors, when the standard deviation of the random error is under 0.05, the algorithm is still robust and can give the accurate temperature field distribution.

Based on this information, the research and development

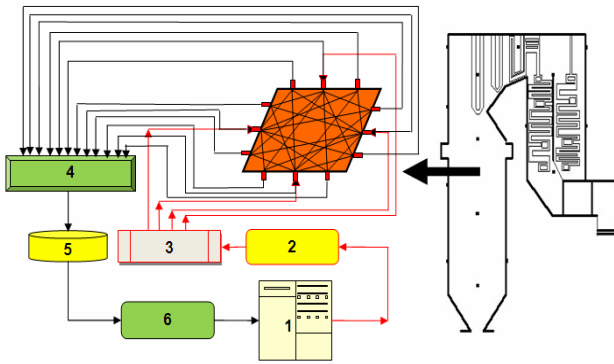
of acoustic pyrometry systems are shown in the following sections.

3. Application and Results

3.1. System Development

The acoustic pyrometry system, which refers to the boiler, acoustics, electronics, computer, digital signal processing, and mechanics, includes acoustic wave generation system, acoustic signal receiving system, data acquisition system and software system. The main devices include an industry control computer (IPC610L) made by Advantech Corporation, the signal generator card (PCI6722) and data acquisition card (PCI 4472) made by National Instruments Corporation, microphones (MPA201) that can be used in an environment with high-temperature and significant levels of dust specially made by BSEA TECH Company in Beijing, power amplifier (MTC 300) and loudspeaker (TORM7300) specially made by Ma Safety Signal Company for the system, and acoustic waveguides designed and manufactured by our laboratory. The software system is implemented with NI labVIEW and Microsoft Visual C++ software programming. Figure 5 presents the flow chart of the system, and Figure 6 shows the main components of the hardware and the interfaces of the software. The whole technological process is as follows: first, digital acoustic signals, which have been sent out by the monitoring software, are converted to analog signals through the sound card. Then, the analog sound signals are amplified by a power amplifier and sent through the loudspeaker on the boiler. After that, the acoustic signals received by the microphones are converted into voltage signals, and then the signals are modulated by the signal conditioning device. At last, the signals, which are acquired through a data collection card in the computer after modulating, can be called by the software. In the

system, the two-dimensional measured cross-section is evenly divided into $4 \times 4 = 16$ pixels, and the temperatures of the 16 pixels are obtained through the regularized reconstruction algorithm. Based on this, the two-dimensional temperature profile of the measured rectangular section can be reconstructed by 16×14 bicubic interpolation. After the operation, the flue gas temperature profile in the furnace will be obtained.



1 Mainframe computer 2 Sound card 3 Power amplifier
4 Signal conditioner 5 Terminal block 6 Data acquisition card

Figure 5. Schematic drawing of system.

The software system, which is a multi-functional, comprehensive and effective management procedure, provides a complete man-machine interface and supports system operation, adjustment and maintenance. The software system is designed with a modular method, including parameter setup, data collection, waveforms display, acoustic emission control, filtering operations, TOF calculation, temperature field visualization, and historical temperature record. All of the functions are automatically completed in the background. Based on object-oriented design and modularization, the system has good maintainability and expandability. When the boiler is running, the operators merely need to see the pictures of the temperature field to know the state of the burning in the boiler furnace. As shown in Figure 6c, the main interface includes tabs that consist of parameter settings, measurement points distribution map, combustion intensity map, 3D display, isotherms, acoustic signal, and frequency spectrum.

In the practical application, the layouts of the measuring points are not only affected by the structure of the boiler, but they are also influenced by the factors of the sound source directivity. On the premise that the tubes of the water wall are not penetrated, there are only the existing viewing ports and soot blower holes that can be used to install acoustic measuring points in the wall of the furnace. Due to the influence of sound source directivity, the measuring points of sound sources should be located in the middle part of the furnace wall to obtain enough SPL (sound pressure level) of the receiving sound.

Figure 1 illustrates the classic layout of measuring points with only one microphone arranged on every point. The microphones and sound sources are numbered from 1 to 8 in

sequence. For instance, microphone 1 is not only used to receive the sound from sound source 1 on point 1 but also to pick up the sound from the other sound sources on the other points. Microphone 1 is close to the sound source 1 with great power, so it needs a large range to meet the requirements. On the other hand, microphone 1 needs high accuracy to acquire the sound from the other sound sources. In the large-scale boiler furnace, due to the strong background noise, a sound source with large power should be used, which makes the range of microphone nearby the source be overstepped, even though it has a large range. Therefore, a special structure is designed for this microphone to lower the received SPL of the nearby sound source, which will influence its accuracy to pick up the signals from other sound sources. Furthermore, the sounds that have gone through the furnace are attenuated so significantly that other microphones cannot receive the signal until its accuracy is improved. The microphones that are used in the system have a hard time meeting the dual requirements of the SPL range (sound source) and signal accuracy (received acoustic signal) at the same time. Therefore, it is difficult to achieve the arrangement shown in Figure 1.

Figure 5 shows a new form of points arrangement in the measuring cross-section unlike that shown in Figure 1, which needs a sound source at every point. In Figure 5, the measuring points of the sound sources, which need microphones with a large range and special structures to lower the SPL function, are arranged in the middle part of the furnace wall. The receiving points of the sound, which need microphones with high accuracy, are installed at two edges of the wall. Then, twelve acoustic points with 4 sound sources are adopted to form 24 paths (see Figure 5) in the system, which has high resolutions of time and space. The linear sweeping frequency signal is used in the acoustic wave generation system, whose frequency is from 500 Hz to 3,000 Hz, and the sweeping cycle is 0.1 s. In this system, the time of flight (TOF), which is the key to realizing acoustic thermometry, can be obtained using the improved generalized correlation method for time delay estimation. The solution of the abovementioned problems, such as time delay estimation, will be discussed in other articles, which are not given here (An et al., 2012). The application of the acoustic pyrometry system in a power plant boiler is described in the following section.

Figure 5 shows a new form of points arrangement in the measuring cross-section unlike that shown in Figure 1, which needs a sound source at every point. In Figure 5, the measuring points of the sound sources, which need microphones with a large range and special structures to lower the SPL function, are arranged in the middle part of the furnace wall. The receiving points of the sound, which need microphones with high accuracy, are installed at two edges of the wall. Then, twelve acoustic points with 4 sound sources are adopted to form 24 paths (see Figure 5) in the system, which has high resolutions of time and space. The linear sweeping frequency signal is used in the acoustic wave generation system, whose frequency is from 500 Hz to 3,000 Hz, and the sweeping cycle is 0.1 s. In this system, the time of flight (TOF), which is the key to realizing acoustic thermometry, can be obtained using

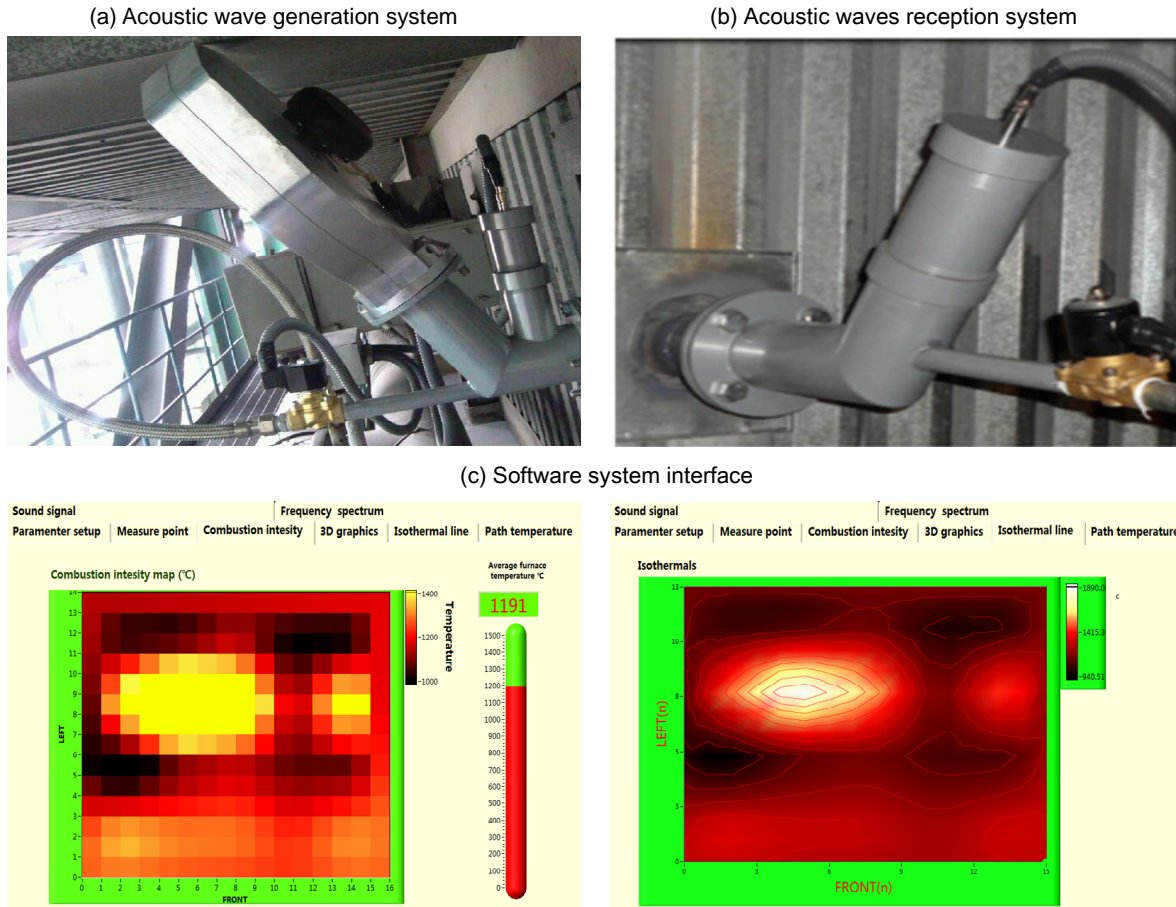


Figure 6. The main components of hardware and the interfaces of software.

the improved generalized correlation method for time delay estimation. The solution of the abovementioned problems, such as time delay estimation, will be discussed in other articles, which are not given here (An et al., 2012). The application of the acoustic pyrometry system in a power plant boiler is described in the following section.

3.2. Application in a Power Plant Boiler

The acoustic pyrometry system was installed in a domestic unit of 300 MW, which had been manufactured by the Babcock & Wilcox Company in Beijing. The rated pressure of steam was 18.4 MPa, and the rated temperature of steam was 543 °C in this boiler.

3.2.1. Measuring Points Arrangement and Exact Lengths of Paths

Without destroying the tubes of the water wall, the measured section was located on a 31 meters high platform in the boiler furnace, which had existing viewing ports and soot blower reserved holes. In view of the actual situation, the acoustic waveguide was adopted to isolate heat, insulate the combustion byproducts, protect the microphones, and amplify

sound like a horn. As shown in Figure 7, the acoustic measuring points were installed in the wall of the furnace. Point 1 was a viewing port in the left wall, point 7 was a viewing port in the right wall, and the other points were soot blower reserved holes. The sound sources were arranged in the middle position of each wall, such as point 2 (sound source 1), point 5 (sound source 2) and point 8 (sound source 3). Because the size of the source device was too large to install under the steel beam in point 11, point 12 (sound source 4) was chosen as the sound source installation point. The microphones with large ranges were installed nearby the sound source, and the microphones with high accuracy were used in the sound reception systems that were installed at point 1, point 3, point 4, point 6, point 7, point 9, point 10 and point 11.

In this way, there were 24 measuring paths formed. After the measuring points were arranged, the acoustic method could be used to measure the exact lengths of the paths, which were difficult to measure by conventional methods. When the boiler was not running, the medium was air like that of the atmospheric environment, and there was no combustion noise in the furnace. Therefore, the lengths could be determined through the measurement of the sound velocity and the TOF. Similarly, two microphones were placed in the furnace 1 m

from each other. A sound source was put nearby one microphone, and an accurate TOF was obtained between the two microphones. The local velocity was 343 m/s. Then, the TOF of the sound wave over the path was measured using the improved generalized cross-correlation method for time delay estimation (An et al., 2012). The distance is easy to obtain, if the speed and time are known. The results shown in Table 1 indicate that the length of the longest measured path achieved was 18 m.

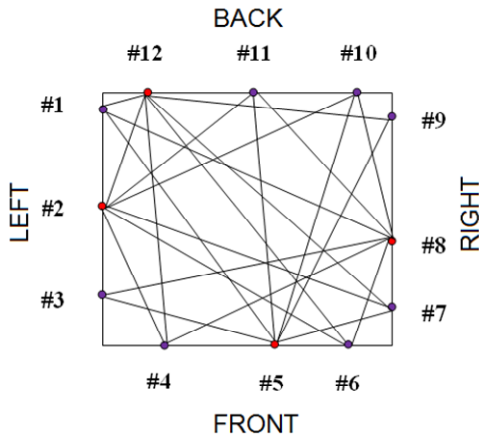


Figure 7. Schematic of measuring point.

3.2.2. Results of Operation

Before temperature measurement, the signals of the background noise were acquired by the microphones when the boiler was running in a hot state. Spectrum feature analysis was conducted to obtain the energy distribution. It was found that the energy of the background noise was mainly distributed in a low frequency band below 600 Hz, and the SPL was between 113 dB and 118 dB, which avoided the main frequencies of the sound source signals. The improved generalized correlation method for time delay estimation, which can reduce the interference of background noise effectively, has been adopted already and is not described here (An et al., 2012).

The type of combustion adopted by the boiler was front wall and back wall opposed firing, and the measured cross-section was above the top burners. Four pairs of burners were symmetrically arranged in the front wall and back wall.

Figure 8 shows the monitoring picture after igniting in which it can be observed that the high temperature regions are on the left side of the profile and close to the front wall due to the combustion instability.

Figure 9 gives the history curves of the unit load and the average temperature of the flue gas in the furnace during 72 hours, which shows that they follow the same trend. Therefore, the temperatures that are measured by acoustic pyrometry can reflect the changes of burning in the furnace.

There are large fluctuations of unit load during another period of time, and the temperatures of the paths are shown in

Figure 10, which illustrates that the temperatures are lower at low load. With the increasing of the load, the temperatures increase and are not steady until the load becomes stable. The trends of all temperatures are the same. Due to the type of combustion, the temperatures of the paths that pass through the high temperature regions near the front wall and the back wall are higher than the paths that go through the regions near the left wall, the right wall and the middle part of profile. When the burning is stable, some monitoring pictures in the hot state are shown in Figure 11. Figure 11a gives the combustion intensity map, which are the temperatures of the 16×14 regions. The temperatures are high in the regions with light color. In contrast, the temperatures are low in the regions with deep color in Figure 11a. Figure 11b shows the three-dimensional temperature display graphics. The abscissa is the size of the temperature profile, and the vertical is the value of the temperature. We can see that there are 8 obvious peaks near the front wall and back wall, and the temperatures in the middle part of the furnace are lower. Figure 11c shows the isotherms, and the regions of high temperatures also use light color. We can also see that the temperatures are higher near the front wall and back wall of the furnace due to the positions of the burners. Figure 11d gives the temperature of the paths. The above are consistent with the mode of the opposed wall firing. In Figure 11a, the average temperature is 1,187 °C.

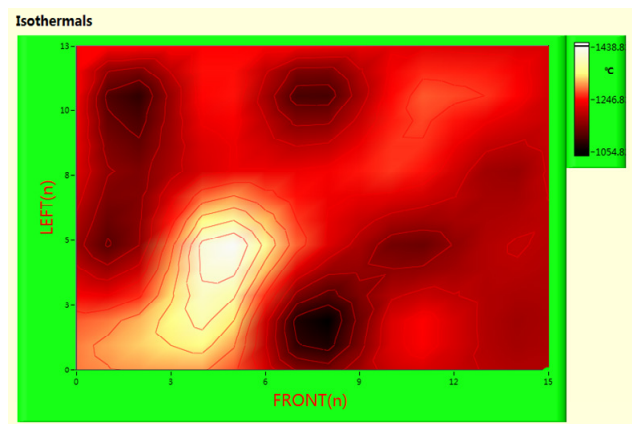


Figure 8. Monitoring picture after igniting.

3.2.3. Temperature Verification

The measured temperature profile is a two-dimensional temperature field, so it cannot be measured by infrared temperature measurement. According to the actual situation, to validate the accuracy of the visualization results that were obtained by the acoustic pyrometry system, thermocouples used in ceramic materials were adopted to measure the temperatures of several regions at the height of 31 m in the furnace. The special thermocouples could accurately measure the temperatures of points in a short time, which were regarded as the actual temperatures of the flue gas. On account of the high temperature in the furnace, the surfaces of the thermocouples

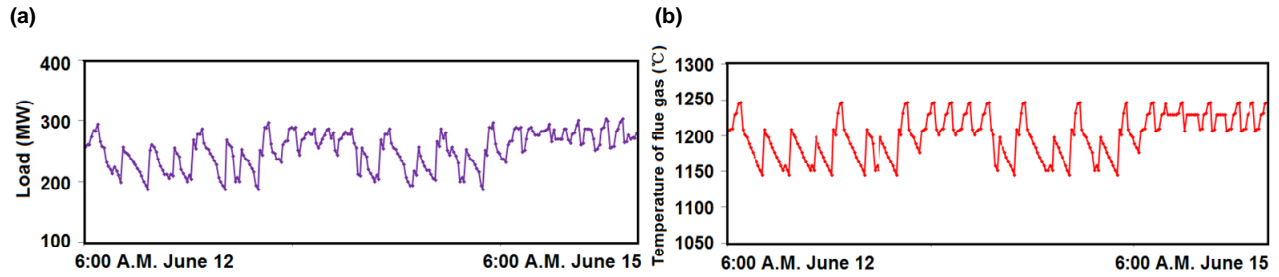


Figure 9. History curves of unit load and the average temperature in the furnace.

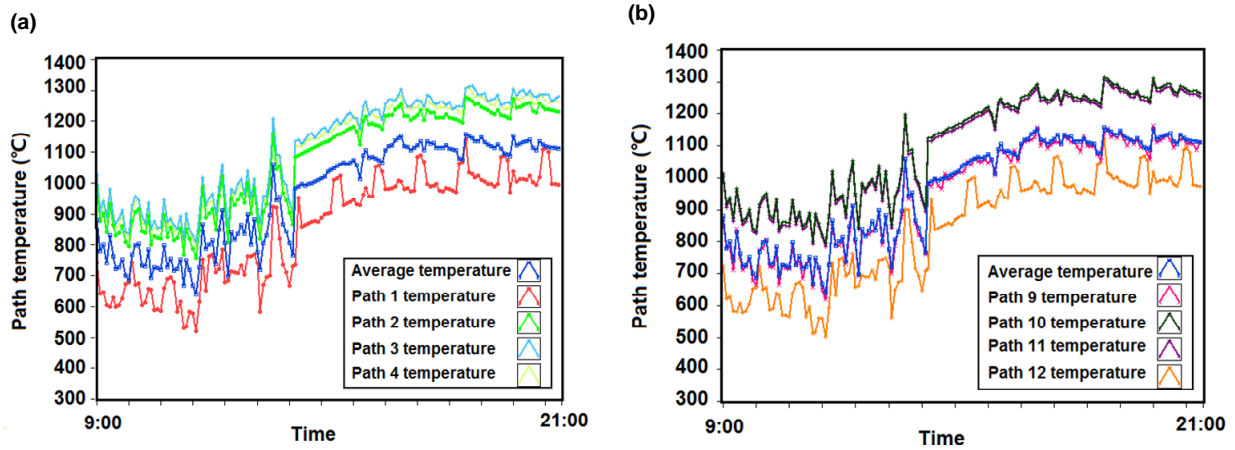


Figure 10. Temperatures of paths.

Table 1. Time of Flight and Lengths of 24 Paths

Serial Number	Paths	TOF/s	L/m	Serial Number	Paths	TOF/s	L/m
1	# 2 - # 4	0.02618	8.980	13	# 8 - # 10	0.02298	7.882
2	# 2 - # 6	0.04688	16.080	14	# 8 - # 11	0.03073	10.540
3	# 2 - # 7	0.04662	15.991	15	# 8 - # 1	0.04786	16.416
4	# 2 - # 9	0.04494	15.414	16	# 8 - # 3	0.04423	15.171
5	# 2 - # 10	0.04197	14.396	17	# 8 - # 4	0.03360	11.525
6	# 2 - # 11	0.02677	9.182	18	# 8 - # 6	0.01483	5.087
7	# 5 - # 7	0.01392	4.775	19	# 12 - # 1	0.00458	1.571
8	# 5 - # 9	0.03739	12.825	20	# 12 - # 3	0.03239	11.110
9	# 5 - # 10	0.03840	13.171	21	# 12 - # 4	0.03836	13.157
10	# 5 - # 11	0.03814	13.082	22	# 12 - # 6	0.05249	18.004
11	# 5 - # 1	0.04650	15.950	23	# 12 - # 7	0.05059	17.352
12	# 5 - # 3	0.03076	10.551	24	# 12 - # 9	0.03919	13.442

Table 2. Measurement Data with Thermo-Couple and Acoustic Pyrometry

Serial number	Thermocouple /°C	Acoustic Pyrometry /°C	Absolute Error /°C	Relative Error /%
1	1,106	1,163	+57	+4.9
2	1,288	1,318	+30	+2.3
3	1,366	1,401	+35	+2.5
4	1,194	1,179	-15	-1.3
5	1,208	1,183	-25	-2.1
6	1,260	1,291	+30	+2.3
7	1,221	1,257	+36	+2.9
8	1,117	1,123	+6	+0.5

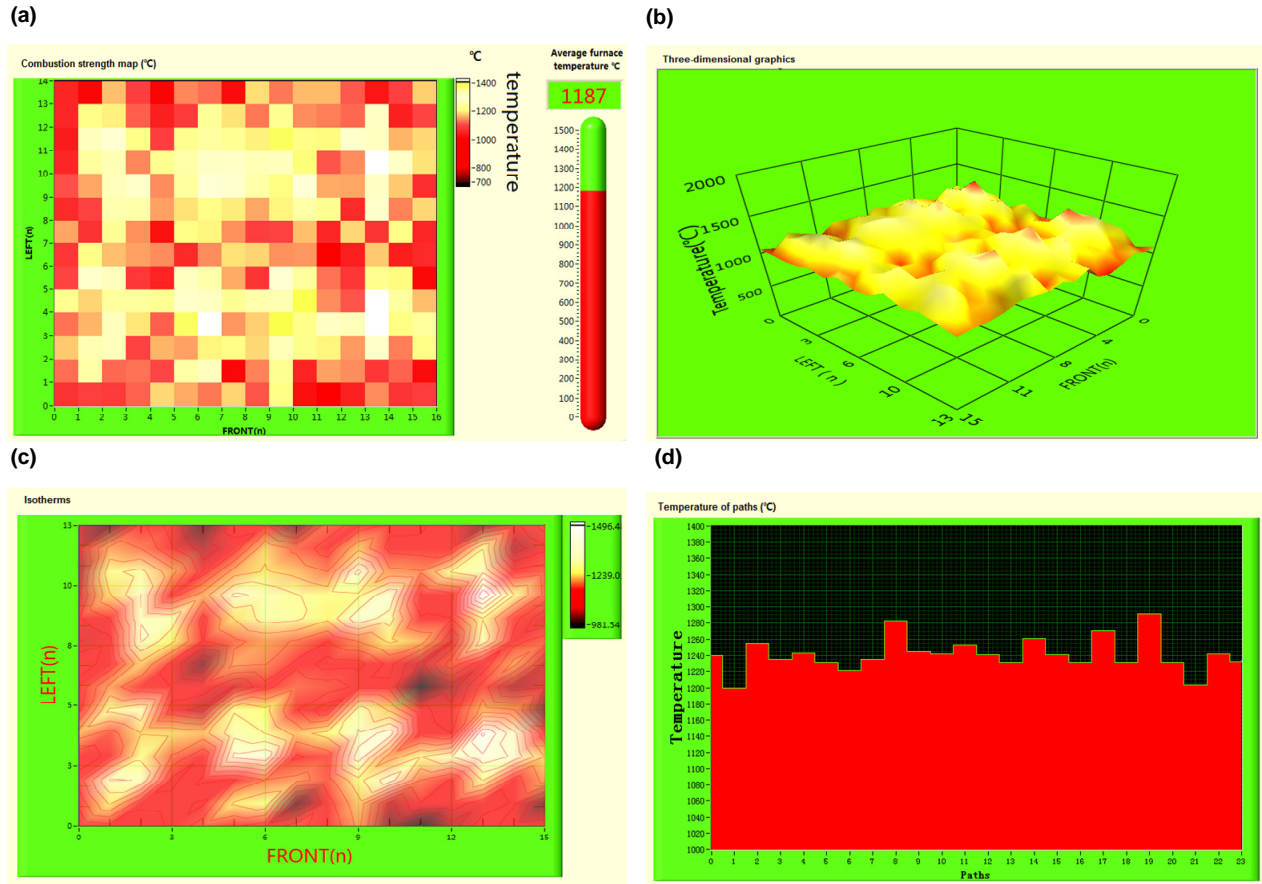


Figure 11. Monitoring pictures in hot state.

would collect ashes and form dregs if they were inserted too deep, which could influence the measurement accuracy. Therefore, the measuring points (1, 2, 3, 4, 5, 6, 7, and 8) were selected to prevent the adverse effects, as shown in Figure 12. The temperatures changed little in every region, so the point temperature represented the region temperature.

The temperatures were measured by the acoustic pyrometry system and thermocouples at the same time, when the unit load was stable at 260 MW. Table 2 gives the measurement results and shows that the relative error is within 5% when using the acoustic pyrometry system, which meets the industry requirements.

4. Conclusions

Using acoustic pyrometry to monitor the temperature field of a boiler furnace, the geometric pixel division and the regularization algorithm were obtained to solve the reconstruction problem. Based on this technique, a monitoring system for the temperature profile through multiple-paths measurements was developed and applied to a 330 MW unit (opposed wall firing). Moreover, successful monitoring of the combustion formed the base of the adjustment in the furnace, which would reduce the environmental pollutants, such as CO and

NOx in the coal-fired power plant. The following conclusions are derived based on the simulation and application experiments:

For the reconstruction of the temperature field, the measured profile was divided into many pixels, and then the typical inverse problem was solved by the regularization algorithm, where the regularization matrix was solved using the adjacent relationship between pixels. The temperatures of the pixels were obtained, and the two-dimensional temperature field was interpolated by bicubic interpolation. The geo-metric pixel division and the regularization algorithm can be used to reconstruct the temperature profile of the boiler furnace in many cases.

Based on electroacoustic source technology, the acoustic pyrometry system, which owned independent intellectual property, was successfully installed and debugged in a domestic 330 MW unit (opposed wall firing). The acoustic pyrometer system could realize the visualization of the temperature profile in the furnace and meet the industry requirements.

Acknowledgments. This research was supported by the Fundamental Research Funds for the Central Universities of China (No. 2014QN 15). We are grateful to the anonymous reviewers whose constructive suggestions have improved the quality of this paper.

References

- An, L. S., Zhang, S. P., Li, G. S., and Shen, G. Q. (2012). Study on time delay estimation in acoustic temperature measurement of power boilers. *J. Chin. Soc. Power Eng.*, 32(3), 197-199.
- Ballester, J., and Garcia-Armingol, T. (2010). Diagnostic techniques for the monitoring and control of practical flames. *Prog. Energy Combust. Sci.*, 36(4), 375-411. <http://dx.doi.org/10.1016/j.peccs.2009.11.005>
- Cai, J. J., Mab, X. Q., and Lic, Q. (2009). On-line monitoring the performance of coal-fired power unit: A method based on support vector machine. *Appl. Therm. Eng.*, 29(11-12), 2308-2319. <http://dx.doi.org/10.1016/j.applthermaleng.2008.11.012>
- Chen, J. H., Hsu, T. Y., Chen, C. C., and Cheng, Y. C. (2010). Monitoring combustion systems using HMM probabilistic reasoning in dynamic flame images. *Appl. Energy*, 87(7), 2169-2179. <http://dx.doi.org/10.1016/j.apenergy.2009.11.008>
- Chi, T. Y., Zhang, H. J., Yan, Y., Zhou, H. L., and Zheng, H. (2010). Investigations into the ignition behaviors of pulverized coals and coal blends in a drop tube furnace using flame monitoring techniques. *Fuel*, 89(3), 743-751. <http://dx.doi.org/10.1016/j.fuel.2009.06.010>
- Doubenskaia, M., Bertrand, P., and Smurov, I. (2006). Pyrometry in laser surface treatment. *Surf. Coatings Technol.*, 201(5), 1955-1961. <http://dx.doi.org/10.1016/j.surfcoat.2006.04.060>
- Feron, P. H. M. (2010). Exploring the potential for improvement of the energy performance of coal fired power plants with post-combustion capture of carbon dioxide. *Int. J. Greenhouse Gas Control*, 4(2), 152-160. <http://dx.doi.org/10.1016/j.ijggc.2009.10.018>
- Frankel, J. I., Keyhani, M., Elkins, B., and Arimilli, R. V. (2010). New in situ method for estimating thermal diffusivity using rate-based temperature sensors. *J. Thermophysics Heat Transfer*, 24(4), 811-817. <http://dx.doi.org/10.2514/1.46300>
- Gam, K. S. (1996). A stable microcomputer-controlled heat pipe furnace and test of new noble metal thermocouples. *Measurement*, 18(2), 101-108. [http://dx.doi.org/10.1016/S0263-2241\(96\)00046-2](http://dx.doi.org/10.1016/S0263-2241(96)00046-2)
- Hoyle, B. S., and Luke, S. P. (1994). Ultrasound in the process industries. *Eng. Sci. Educ. J.*, 3(3), 119-122. <http://dx.doi.org/10.1049/esej:19940309>
- Jen, C. K., Legoux, J. G., and Parent, L. (2000). Experimental evaluation of clad metallic buffer rods for high temperature ultrasonic measurements. *NDT & E Int.*, 33(3), 145-153. [http://dx.doi.org/10.1016/S0963-8695\(99\)00042-0](http://dx.doi.org/10.1016/S0963-8695(99)00042-0)
- Keys, R. G. (1981). Cubic convolution interpolation for digital image processing. *IEEE Trans. Acoust. Speech Signal Process.*, 29(6), 1153-1160. <http://dx.doi.org/10.1109/TASSP.1981.1163711>
- Konno, M., Cui, A., Nishiwaki, N., and Hori, S. (1993). Measurement of the polymer melt temperature in injection molding machine by using ultrasonic technique. *Proc. of the 51st Annual Technical Conference*, Society of Plastics Engineers, New Orleans, LA, USA. pp. 2798-2803.
- Liu, T., Fernando, G. F., Zhang, Z. Y., and Grattan, K. T. V. (2000). Simultaneous strain and temperature measurements in composites using extrinsic Fabry-Perot interferometric and intrinsic rare-earth doped fiber sensors. *Sensors Actuators A: Phys.*, 80 (3), 208-215. [http://dx.doi.org/10.1016/S0924-4247\(99\)00309-X](http://dx.doi.org/10.1016/S0924-4247(99)00309-X)
- Mahan, J. R., and Yeater, K. M. (2008). Agricultural applications of a low-cost infrared thermometer. *Comput. Electron. Agric.*, 64(2), 262-267. <http://dx.doi.org/10.1016/j.compag.2008.05.017>
- Meriaudeau, F. (2007). Real time multispectral high temperature measurement: Application to control in the industry. *Image Vision Comput.*, 25(7), 1124-1133. <http://dx.doi.org/10.1016/j.imavis.2006.04.019>
- Moll, J., Schulte, R. T., Fritzen, C.-P., and Nelles, O. (2010). Multi-site damage localization in anisotropic plate-like structures using an active guided wave structural health monitoring system. *Smart Mater. Struct.*, 19(4), 1-16. <http://dx.doi.org/10.1088/0964-1726/19/4/045022>
- Myers, M. R., Jorge, A. B., Yuhast, D. E., and Walker, D. G. (2013). Using ultrasound and the extended kalman filter for characterizing aerothermodynamic environments. *AIAA J.*, 51(10), 2410-419. <http://dx.doi.org/10.2514/1.J052313>
- Pedersen, K. H., Jensen, A. D., Berg, M., Olsen, L. H., and Dam-Johansen, K. (2009). The effect of combustion conditions in a full-scale low-NOx coal fired unit on fly ash properties for its application in concrete mixtures. *Fuel Process. Technol.*, 90 (2), 180-185. <http://dx.doi.org/10.1016/j.fuproc.2008.08.012>
- Popp, D. (2010). Exploring links between innovation and diffusion: adoption of NOx control technologies at US coal-fired power plants. *Environ. Resour. Econ.*, 45(3), 319-352. <http://dx.doi.org/10.1007/s10640-009-9317-1>
- Pullins, C. A., and Diller, T. E. (2010). In situ high temperature heat flux sensor calibration. *Int. J. Heat Mass Transfer*, 53(17-18), 3429-3438. <http://dx.doi.org/10.1016/j.ijheatmasstransfer.2010.03.042>
- Ranc, N., and Wagner, D. (2005). Some aspects of Portevin-Le Châtelier plastic instabilities investigated by infrared pyrometry. *Mater. Sci. Eng. A*, 394(1-2), 87-95. <http://dx.doi.org/10.1016/j.msea.2004.11.042>
- Reginska, T. (1996). A regularization parameter in discrete ill-posed problems. *SIAM J. Sci. Comput.*, 17(3), 740-749. <http://dx.doi.org/10.1137/S1064827593252672>
- Romero, C., Li, X., Keyvan, S., and Rossow, R. (2005). Spectrometer-based combustion monitoring for flame stoichiometry and temperature control. *Appl. Therm. Eng.*, 25(5-6), 659-676. <http://dx.doi.org/10.1016/j.applthermaleng.2004.07.020>
- Sarma, U., and Boruah, P. K. (2010). Design and development of a high precision thermocouple based smart industrial thermometer with on line linearisation and data logging feature. *Measurement*, 43(10), 1589-1594. <http://dx.doi.org/10.1016/j.measurement.2010.09.003>
- Seat, H. C., Sharp, J. H., Zhang, Z. Y., and Grattan, K. T. V. (2002). Single-crystal ruby fiber temperature sensor. *Sensors Actuators A: Phys.*, 101(1-2), 24-29. [http://dx.doi.org/10.1016/S0924-4247\(02\)00190-5](http://dx.doi.org/10.1016/S0924-4247(02)00190-5)
- Srinivasan, K., Sundararajan, T., Narayanan, S., Jothi, T. J. S., and Rohit Sarma, C. S. L. V. (2013). Acoustic pyrometry in flames. *Measurement*, 46(1), 315-323. <http://dx.doi.org/10.1016/j.measurement.2012.07.003>
- Tarantola, A. (1987). Inverse problem theory-methods for data fitting and model parameter estimation, *Elsevier Science Publisher BV*, pp. 1-10.
- Thitakamol, B., Veawab, A., and Aroonwilas, A. (2007). Environmental impacts of absorption-based CO2 capture unit for post-combustion treatment of flue gas from coal-fired power plant. *Int. J. Greenhouse Gas Control*, 1(3), 318-342. [http://dx.doi.org/10.1016/S1750-5836\(07\)00042-4](http://dx.doi.org/10.1016/S1750-5836(07)00042-4)
- Wadley, H. N. G., Norton, S. J., Mauer, F., Drone, B., Ash, E. A., and Sayers, C. M. (1986). Ultrasonic measurement of internal temperature distribution. *Philos. Trans. Roy. Soc. London. Ser. A.*, 320(1554), 341-361. <http://dx.doi.org/10.1098/rsta.1986.0123>
- Walker, D. G., Scott, E. P., and Nowak, R. J. (2000). Estimation methods for two-dimensional conduction effects of shock-shock heat fluxes. *J. Thermophysics Heat Transfer*, 14(4), 533-539. <http://dx.doi.org/10.2514/2.6554>
- Wang, N. L., Zhang, Y., Zhang, T., and Yang, Y. P. (2012). Data mining-based operation optimization of large coal-fired power plants. *AASRI Procedia*, 3, 607-612. <http://dx.doi.org/10.1016/j.aasri.2012.11.096>

- Yan, H., Chen, G. N., Zhou, Y. G., and Liu, L. J. (2012). Primary study of temperature distribution measurement in stored grain based on acoustic tomography. *Exp. Therm. Fluid Sci.*, 42, 55-63. <http://dx.doi.org/10.1016/j.expthermflusci.2012.04.010>
- Yan, Y., Lu, G., and Colechin, M. (2002). Monitoring and characterisation of pulverised coal flames using digital imaging techniques. *Fuel*, 81(5), 647-655. [http://dx.doi.org/10.1016/S0016-2361\(01\)00161-2](http://dx.doi.org/10.1016/S0016-2361(01)00161-2)
- Yu, M., Särner, G., Luijten, C. C. M., Richter, M., Aldén, M., and Baert, R. S. G. (2010). Survivability of thermographic phosphors (YAG: Dy) in a combustion environment. *Measur. Sci. Technol.*, 21(3), 1-4. <http://dx.doi.org/10.1088/0957-0233/21/3/037002>
- Zhao, Y., Wang, S. X., Duan, L., Lei, Y., Cao, P. F., and Hao, J. M. (2008). Primary air pollutant emissions of coal-fired power plants in China: Current status and future prediction. *Atmos. Environ.*, 42(36), 8442-8452. <http://dx.doi.org/10.1016/j.atmosenv.2008.08.021>
- Zhao, Y., Wang, S. X., Nielsen, C. P., Li, X. H., and Hao, J. M. (2010). Establishment of a database of emission factors for atmospheric pollutants from Chinese coal-fired power plants. *Atmos. Environ.*, 44(12), 1515-1523. <http://dx.doi.org/10.1016/j.atmosenv.2010.01.017>
- Zhu, X. P., Rizzo, P., Marzani, A., and Bruck, J. (2010). Ultrasonic guided waves for nondestructive evaluation/structural health monitoring of trusses. *Measur. Sci. Technol.*, 21(4), 1-12. <http://dx.doi.org/10.1088/0957-0233/21/4/045701>